Effective actions for the $SU(2)$ confinement-deconfinement phase transition

Thomas Heinzl*

School of Mathematics and Statistics, University of Plymouth, Drake Circus, Plymouth, PL4 8AA, United Kingdom

Tobias Kaestner† and Andreas Wipf‡

Theoretisch-Physikalisches Institut, Friedrich-Schiller-Universität Jena, Max-Wien-Platz 1, 07743 Jena, Germany

(Received 4 April 2005; published 8 September 2005)

We compare different Polyakov-loop actions yielding effective descriptions of finite-temperature $SU(2)$ Yang-Mills theory on the lattice. The actions are motivated by a simultaneous strong coupling and character expansion obeying center symmetry and include both Ising and Ginzburg-Landau type models. To keep things simple we limit ourselves to nearest-neighbor interactions. Some truncations involving the most relevant characters are studied within a novel mean-field approximation. Using inverse Monte Carlo techniques based on exact *geometrical* Schwinger-Dyson equations we determine the effective couplings of the Polyakov-loop actions. Monte Carlo simulations of these actions reveal that the mean-field analysis is a fairly good guide to the physics involved. Our Polyakov-loop actions reproduce standard Yang-Mills observables well up to limitations due to the nearest-neighbor approximation.

DOI: 10.1103/PhysRevD.72.065005 PACS numbers: 11.10.Wx, 11.15.Ha, 11.15.Me

I. INTRODUCTION

The finite-temperature confinement-deconfinement phase transition in $SU(2)$ Yang-Mills theory originally conjectured by Polyakov [1] and Susskind [2] is by now fairly well established. The order parameter is the Polyakov loop,

$$L_{\boldsymbol{x}} \equiv \frac{1}{2}\,\mathrm{tr}\mathcal{T}\exp\Big(i\int_0^{\beta_T} d\tau A^0(\boldsymbol{x},\tau)\Big), \tag{1}$$

a traced Wilson line that winds around the periodic Euclidean time direction parameterized by τ, $0 \le \tau \le \beta_T$ where $\beta_T = 1/T$ is the inverse temperature. In the confined phase the expectation value $\langle L\rangle$ is zero, while it becomes nonvanishing in the broken, deconfined phase. The Polyakov loop transforms nontrivially under the center symmetry,

$$L_{\boldsymbol{x}} \to zL_{\boldsymbol{x}}, \qquad z = \pm 1 \in \mathbb{Z}(2). \tag{2}$$

Thus, above the critical temperature, $T = T_c$, this symmetry becomes spontaneously broken. Lattice calculations have shown beyond any doubt that the phase transition is second order with the critical exponents being those of the $3d$ Ising model [3–6]. This is in accordance with the Svetitsky-Yaffe conjecture [7,8] which states, in particular, that $SU(2)$ Yang-Mills theory (in $4d$) is in the universality class of a $\mathbb{Z}(2)$ spin model (in $3d$) with short-range interactions. Hence, it should be possible to describe the confinement-deconfinement transition by an effective theory formulated solely in terms of the Polyakov loop $L_{\boldsymbol{x}}$. The most general ansatz is given by a center–symmetric effective Polyakov-loop action (PLA) of the form [9]

$$S_{\mathrm{PL}}[L] = \sum_{\boldsymbol{x}} V[L_{\boldsymbol{x}}^2] + \sum_{\boldsymbol{xy}} L_{\boldsymbol{x}} K^{(2)}_{\boldsymbol{xy}} L_{\boldsymbol{y}} + \sum_{\boldsymbol{xyuv}} L_{\boldsymbol{x}} L_{\boldsymbol{y}} K^{(4)}_{\boldsymbol{xyuv}} L_{\boldsymbol{u}} L_{\boldsymbol{v}} + \ldots. \tag{3}$$

There is a potential term V, a power series in $L_{\boldsymbol{x}}^2$ living on single lattice sites $\boldsymbol{x}$, plus hopping terms with kernels $K^{(2n)}$ connecting more and more lattice sites $\boldsymbol{x}, \boldsymbol{y}, \ldots$. It is important to note that L is a dimensionless and compact variable, $L_{\boldsymbol{x}} \in [-1, 1]$. Thus, in principle, one is confronted with a proliferation of possible operators that may appear in the PLA (3). One simplification arises due to the Svetitsky-Yaffe conjecture implying that the kernels $K^{(2n)}$ should be short ranged. Hence, upon expanding like for instance,

$$K^{(2)}_{\boldsymbol{xy}} = \sum_{\boldsymbol{r}} \lambda_{\boldsymbol{r}} \delta_{\boldsymbol{y},\boldsymbol{x}+\boldsymbol{r}}, \tag{4}$$

one expects that the first few terms with small $r \equiv |\boldsymbol{x} - \boldsymbol{y}|$ will dominate, i.e. will have the largest couplings λ_r. To check this expectation one needs a reliable method to calculate the kernels $K^{(2n)}$ or, equivalently, the coupling parameters inherent in them. A particularly suited approach is introduced in the following section.

II. INVERSE MONTE CARLO METHOD

Inverse Monte Carlo (IMC) is a numerical method to determine effective actions [10–12]. The latter are generically defined via

$$\exp(-S_{\mathrm{eff}}[X]) \equiv \int \mathfrak{D}U\,\delta(X - X[U])\exp(-S[U]), \tag{5}$$

where the U's represent some "microscopic" degrees of freedom and the X's the effective "macroscopic" ones. In the spirit of Wilson's renormalization group, these are obtained by integrating out the U's in favor of the X's. It

*Electronic address: theinzl@plymouth.ac.uk
†Electronic address: kaestner@tpi.uni-jena.de
‡Electronic address: wipf@tpi.uni-jena.de

is important to distinguish this "Wilsonian" notion of an effective action from the 1-particle-irreducible (1PI) effective action which will later on be employed as well (cf. the recent remarks in [13]).

Of course, the problem with (5) is to do the integration nonperturbatively which in general is not possible. In this case, one has to resort to choosing an ansatz like (3) as dictated by symmetry and dimensional counting or to do the integration numerically. The huge number of degrees of freedom involved clearly suggests to use Monte Carlo (MC) methods. However, this amounts to calculating expectation values rather than integrals like (5). Hence, one needs a recipe to get *from expectation values to effective actions*. This is exactly what IMC is supposed to do (see Fig. 1).

Our particular IMC method is based on the Schwinger-Dyson equations that must hold in the effective theory once a particular ansatz is chosen [11,12] (for an alternative see [10]). In our case, the macroscopic degrees are given by the Polyakov loops $L_{\boldsymbol{x}}$ distributed according to the PLA (3) which we rewrite as

$$S_{\mathrm{PL}}[L] \equiv \sum_{a=1}^{N_a} \lambda_a S_a[L], \tag{6}$$

with $\mathbb{Z}(2)$ symmetric operators S_a and coupling parameters λ_a to be determined from the Schwinger-Dyson equations. To derive these, we proceed as follows.

On a lattice with spacing a and temporal extent N_t (hence temperature $T = 1/N_t a$) the Polyakov line is given by the product of temporal links,

$$\mathfrak{P}_{\boldsymbol{x}} \equiv \prod_{t=1}^{N_t} U_{\boldsymbol{x},t;0} \in SU(2). \tag{7}$$

This $SU(2)$ matrix may be diagonalized whereupon it can be written as

$$\mathfrak{P}_{\boldsymbol{x}} = \begin{pmatrix} \exp(i\theta_{\boldsymbol{x}}) & 0 \\ 0 & \exp(-i\theta_{\boldsymbol{x}}) \end{pmatrix},$$

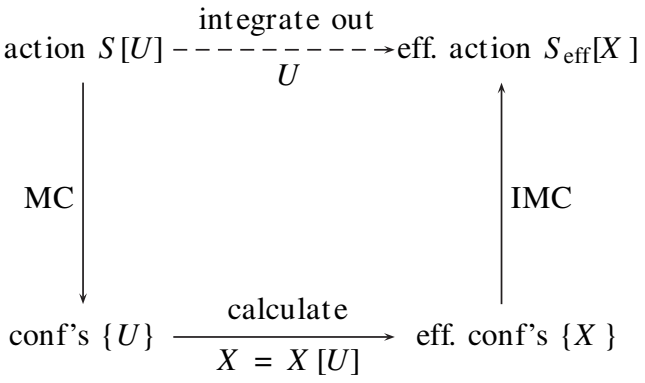

FIG. 1. Illustration of the IMC procedure.

with $-\pi \le \theta_{\boldsymbol{x}} \le \pi$. This representation immediately yields the trace (divided by two),

$$L_{\boldsymbol{x}} = \frac{1}{2}\,\mathrm{tr}\mathfrak{P}_{\boldsymbol{x}} = \cos\theta_{\boldsymbol{x}}, \tag{8}$$

which contains all the gauge invariant information contained in the group variable $\mathfrak{P}_{\boldsymbol{x}}$. As an aside, we remark that this peculiar feature will no longer be true for higher $SU(N)$ groups [14,15]. In this more general case, traces of $N-1$ different powers of $\mathfrak{P}$ are required.

With (5) the action (6) leads to the partition function

$$Z = \int \mathfrak{D}L \exp(-S_{\mathrm{PL}}[L]), \tag{9}$$

where the integration is performed with the reduced Haar measure h of $SU(2)$,

$$DL \equiv \prod_{\boldsymbol{x}} dh(L_{\boldsymbol{x}}), \qquad dh(u) = \frac{2}{\pi}\sqrt{1-u^2}\,du. \tag{10}$$

Since S_{PL} depends on the Polyakov loop only via the class function $L_{\boldsymbol{x}}$ in (8) we may use the left-right invariant Haar measure $D\mathfrak{P}$ in (9) instead of the reduced Haar measure. The enhanced symmetry of the measure yields the following *geometrical* Schwinger-Dyson equations [16],

$$0 = \int \mathfrak{D}L \exp(-S_{\mathrm{PL}})[3L_{\boldsymbol{x}}G - (1-L_{\boldsymbol{x}}^2)(G'_{\boldsymbol{x}} - GS'_{\mathrm{PL},\boldsymbol{x}})]. \tag{11}$$

Here, $G[L]$ represents some set of functions of the Polyakov loop to be chosen appropriately (see below). In addition, we have defined the derivative $G'_{\boldsymbol{x}} \equiv \partial G/\partial L_{\boldsymbol{x}}$ and analogously for S_{PL}.

Switching to expectation value notation, (11) can be rewritten as a linear system for the couplings in (6),

$$\sum_a \langle (1-L_{\boldsymbol{x}}^2) G S'_{a,\boldsymbol{x}} \rangle \lambda_a = \langle (1-L_{\boldsymbol{x}}^2) G'_{\boldsymbol{x}} \rangle - 3\langle L_{\boldsymbol{x}} G \rangle. \tag{12}$$

The coefficients of this system are expectation values which are calculated in the full Yang–Mills ensemble obtained by MC simulation based on the $SU(2)$ Wilson action. Numerically, it is of advantage to have more equations than unknown couplings λ_a. This is achieved by choosing G out of the following set of local functions,

$$G_{a,\boldsymbol{y}} \in \{\partial S_a/L_{\boldsymbol{y}}, a = 1, \ldots, N_a\}, \tag{13}$$

which represent the operators present in the equation of motion for $L_{\boldsymbol{y}}$. For *fixed* $\boldsymbol{y}$, (12) then yields as many equations as there are couplings, namely N_a. These equations relate different two-point functions labeled by lattice sites $\boldsymbol{x}$ and $\boldsymbol{y}$ of distance r. Additional relations are obtained by letting the distance r run through (half of) the spatial lattice extent, $r = 1, \ldots, N_s/2$. Altogether, the overdetermined system (12) consists of $N_a \times N_s/2$ equations which are solved by least-square methods. We would like to stress that having more equations than unknowns

(by a factor $N_s/2$) together with the special choice (13) greatly enhances the stability of the IMC algorithm. In particular, we do not encounter any ill-conditioned matrices. For more details the reader is referred to Appendix B and [16].

III. CHARACTER EXPANSION

To find a reasonable choice of operators for the ansatz (6) we use the beautiful analytical results of Billó *et al.* [17]. These authors have evaluated the integral (5) for the case at hand ($S[U]$ being the Wilson action, $X \equiv L$ the Polyakov loop) by combining the strong coupling with a character expansion. For the benefit of the reader we briefly recapitulate their approach before we adopt it for our purposes.

Recall that a character is the trace of a group element in an irreducible representation. If j denotes the spin of an $SU(2)$ representation such that $p = 2j$ is the length of the corresponding Young tableau, then the associated character is

$$\chi_p(U) = \mathrm{tr}_p(U) = \frac{\sin((p+1)\theta)}{\sin\theta}, \qquad p = 0, 1, 2, \ldots. \tag{14}$$

The characters can be entirely expressed as orthogonal polynomials in the traced loop L, namely, the Chebyshev polynomials of the second kind [18],

$$\chi_p(U) = \sum_{k=0}^{[p/2]} \frac{(-1)^k (p-k)!}{k!(p-2k)!} (2L)^{p-2k}.$$

This representation manifestly shows that χ_p is a polynomial in L of order p. The first few characters are

$$\chi_0 = 1, \qquad \chi_1 = 2L, \qquad \chi_2 = 4L^2 - 1, \qquad \chi_3 = 8L^3 - 4L. \tag{15}$$

To determine the PLA S_{PL} (6) in the strong-coupling limit of the underlying $SU(2)$ gauge theory Billó *et al.* [17] allowed for different couplings in temporal and spatial directions, denoted β_t and β_s, respectively. In terms of these couplings the original Wilson coupling becomes

$$\beta = \frac{4}{g^2} = \sqrt{\beta_t \beta_s}.$$

The formula for the temperature,

$$T = \frac{1}{N_t} \sqrt{\frac{\beta_t}{\beta_s}},$$

shows that the high-temperature limit (for β_t fixed) corresponds to N_t or β_s being small. An expansion in terms of β_s results in the PLA [17]

$$S_{\mathrm{PL}} \equiv \sum_{\langle xy \rangle} \log\left\{1 + \sum_{p=1}^{\infty} \kappa_p \chi_p(L_x) \chi_p(L_y)\right\} + \ldots \tag{16}$$

where all orders in β_t have been summed up in terms of coupling coefficients $\kappa_p = \kappa_p(\beta_t)$. The terms not written explicitly contain higher orders in β_s and interactions of characters of plaquette type. The leading-order action (16) involves only *nearest-neighbor* (NN) interactions with the couplings given explicitly by

$$\kappa_p(\beta_t) = -\left[\frac{I_{p+1}(\beta_t)}{I_1(\beta_t)}\right]^{N_t}. \tag{17}$$

Asymptotically, for small β_t, this is

$$\kappa_p = -c_p \beta_t^{pN_t} + O(\beta_t^{pN_t+2}), \qquad c_p \equiv [2^p (p+1)!]^{-N_t}. \tag{18}$$

This concludes our brief discussion of [17]. In order to make the operator (i.e. character) content of the action (16) more explicit we expand the log in (16) in powers of β_t. From the small-β_t behavior (18), we infer that a product of n κ's behaves as

$$\kappa_{p_1} \ldots \kappa_{p_n} = O(\beta_t^{pN_t}), \qquad p \equiv \sum_{i=1}^{n} p_i. \tag{19}$$

Thus we reshuffle the expansion of (16) such that, for fixed p, we first sum over all partitions of the integer p, then increase p by one unit, sum again etc. up to some maximal value, say $p = 3$. In this way we obtain

$$S_{\mathrm{PL}} = S^{(1)} + S^{(2)} + S^{(3)} + O(\beta_t^{4N_t}), \tag{20}$$

where $S^{(p)}$ is $O(\beta_t^{pN_t})$. Accordingly, we have a hierarchy of actions $S^{(p)}$ that become more and more suppressed (for small β_t) as p increases. We thus refer to $S^{(1)}$ as being of leading order (LO), $S^{(2)}$ of next-to-leading order (NLO) and so on. Abbreviating $\chi_{px} = \chi_p(L_x)$ the actions $S^{(p)}$ read explicitly

$$S^{(1)} = \sum_{\langle xy \rangle} \kappa_1 \chi_{1x} \chi_{1y},$$

$$S^{(2)} = \sum_{\langle xy \rangle} \left(\kappa_2 \chi_{2x} \chi_{2y} - \frac{1}{2} \kappa_1^2 \chi_{1x}^2 \chi_{1y}^2\right),$$

$$S^{(3)} = \sum_{\langle xy \rangle} \left(\kappa_3 \chi_{3x} \chi_{3y} - \kappa_1 \kappa_2 \chi_{1x} \chi_{2x} \chi_{1y} \chi_{2y} + \frac{1}{3} \kappa_1^3 \chi_{1x}^3 \chi_{1y}^3\right).$$

The product of characters at the *same site* may be further reduced by the $SU(2)$ "reduction formula,"

$$\chi_{p_1} \chi_{p_2} = \chi_{p_1+p_2} + \chi_{p_1+p_2-2} + \ldots + \chi_{|p_1-p_2|}.$$

Note that our conventions are such that the subscripts get reduced by two units from left to right. Using this formula

in the above expressions we end up with

$$S^{(1)} = \sum_{\langle xy\rangle} \lambda_{11}^{(1)} \chi_{1x}\chi_{1y}, \tag{21}$$

$$S^{(2)} = \sum_{\langle xy\rangle} \lambda_{22}^{(2)} \chi_{2x}\chi_{2y} + 2d\sum_{x} \lambda_{20}^{(2)} \chi_{2x}, \tag{22}$$

$$S^{(3)} = \sum_{\langle xy\rangle} [\lambda_{11}^{(3)} \chi_{1x}\chi_{1y} + \lambda_{33}^{(3)} \chi_{3x}\chi_{3y} + \lambda_{13}^{(3)} (\chi_{1x}\chi_{3y} + \chi_{3x}\chi_{1y})]. \tag{23}$$

The new couplings λ_{pq} are combinations of the κ's, namely

$$\lambda_{11}^{(1)} = \kappa_1, \qquad \lambda_{11}^{(3)} = -\kappa_1\kappa_2 + \frac{4}{3}\kappa_1^3, \tag{24}$$

$$\lambda_{22}^{(2)} = \kappa_2 - \frac{1}{2}\kappa_1^2, \qquad \lambda_{02}^{(2)} = -\frac{1}{2}\kappa_1^2, \tag{25}$$

$$\lambda_{33}^{(3)} = \kappa_3 - \kappa_1\kappa_2 + \frac{1}{3}\kappa_1^3, \tag{26}$$

$$\lambda_{13}^{(3)} = -\kappa_1\kappa_2 + \frac{2}{3}\kappa_1^3. \tag{27}$$

In the asymptotic regime, $\beta_t \ll 1$, the λ's may be expanded with the help of (18) (see Sec. V below). The results (21)–(23) from combining character and strong-coupling expansion suggest the following ansatz for the PLA,

$$S_{\mathrm{PL}} = \sum_{\langle xy\rangle,(pq)} \lambda_{pq}\chi_{px}\chi_{qy} \equiv \sum_{(pq)} S_{pq}. \tag{28}$$

The couplings λ_{pq} are symmetric with respect to their indices pq, and $p - q$ is even. The ansatz (31) coincides with the one suggested by Dumitru et al. [15] which was entirely based on center symmetry. It is obvious that the action (31) is center-symmetric as the χ_p are even/odd functions for p even/odd, $\chi_p(-L) = (-1)^p\chi_p(L)$.

The terms which product $pq = 0$ are localized at single sites and correspond to ''potentials''. Hence the action splits into hopping terms T and potential terms V in accordance with (3),

$$S_{\mathrm{PL}} = \sum_{\substack{(pq)\\ pq\neq 0}} S_{pq} + 2\sum_{p} S_{p0} \equiv T + V. \tag{29}$$

With $\chi_0 = 1$ the potential V has the explicit form

$$V = 2d \sum_{p\ \mathrm{even}} \lambda_{0p}\sum_{x} \chi_{px}. \tag{30}$$

For what follows we need some notation. We will, of course, truncate our actions at some maximum ''spin'' p, say at $p = r$. Thus we define the truncated actions

$$S_r \equiv \sum_{(pq)}^{r} S_{pq} = \sum_{\substack{(pq)\\ pq\neq 0}}^{r} S_{pq} + 2\sum_{p=2}^{r} S_{p0} \equiv T_r + V_r, \tag{31}$$

where all summations are cut off at $p = r$. Explicitly, the first few terms are

$$S_1 = S_{11}, \tag{32}$$

$$S_2 = (S_{11} + S_{22}) + 2S_{20} \equiv T_2 + V_2, \tag{33}$$

$$S_3 = (T_2 + S_{31} + S_{33}) + 2S_{20} \equiv T_3 + V_3. \tag{34}$$

Note that actually $V_3 = V_2$. In the strong-coupling expansion the action S_r is of order $O(\beta^{rN_t})$. As before, we refer to $p = 1$ (fundamental representation) as the LO, to $p = 2$ (adjoint representation) as NLO and so on. In this paper we will not go beyond $p = 3$, a truncation that neglects terms which are NNNLO in the strong-coupling expansion.

According to (36) the first potential term arising in the strong-coupling character expansion is of NLO (β^{2N_t}) and quadratic in the Polyakov-loop L,

$$V_2 = 2d\lambda_{02}\sum_{x} \chi_{2x}. \tag{35}$$

IV. MEAN-FIELD APPROXIMATION

A. Generalities

Before we actually relate the PLAs (31) to Yang-Mills theory let us analyze their critical behavior which is interesting in itself. Both via mean-field (MF) analysis and MC simulation we will see that the models typically have a second order phase transition at certain critical couplings. Obviously, this should match with the Yang-Mills critical behavior.

The models involving more than a single hopping term also show a first-order transition at which the order parameter $\langle L\rangle$ jumps. For the $SU(2)$ case discussed here this transition is not related to Yang-Mills. Matching to the latter hence implies that the effective couplings should stay away from the first-order critical surface.

To develop a MF approximation for the Polyakov loop L with its nontrivial target space $[-1, 1]$ we use a variational approach based on the text [19]. Our starting point is the *effective action* Γ for the Polyakov-loop dynamics. This time, the term ''effective action'' refers to the generating functional for the 1PI correlators of the Polyakov loop. The former represents the complete information of the quantum field theories based on the PLAs S_{PL}. This is obvious from the fact that Γ is the Legendre transform of the Schwinger functional W,

$$\Gamma[\bar{L}] = (\mathfrak{L}W)[\bar{L}], \qquad W[J] = \log Z[J], \tag{36}$$

$$Z[J] = \int \mathfrak{D}L \exp(-S_{\mathrm{PL}}[L] + (J, L)). \tag{37}$$

These are the standard definitions to be found in any text book on quantum field theory. For an alternative, variational characterization of Γ [19] we consider the following *probability measures* on field space,

$$d\mu[L] = \mathfrak{D}L\, p[L], \tag{38}$$

with nonnegative function $p[L]$ and $\mathfrak{D}L$ as in (10). Averages are calculated with μ. For example, the mean PLA is

$$\langle S_{\mathrm{PL}}\rangle_\mu = \int d\mu[L] S_{\mathrm{PL}}[L], \tag{39}$$

while the Boltzmann-Gibbs-Shannon entropy is given by the average of $\log p$,

$$S_{\mathrm{BGS}}[\mu] \equiv -\langle \log p\rangle_\mu = -\int d\mu[L] \log p[L]. \tag{40}$$

The relevant variational principles are obtained as follows. By subtracting (40) from (39) one forms

$$F[\mu] \equiv \langle S_{\mathrm{PL}} + \log p\rangle_\mu \equiv F[p]. \tag{41}$$

This analog of the free energy is varied with respect to p under appropriately chosen constraints. These are added via Lagrange multipliers. If one just requires normalization to unity, $\langle 1\rangle_\mu = 1$, one finds that the probability p for which (41) becomes extremal is given by the standard measure, $p = \exp(-S_{\mathrm{PL}})/Z[0]$. Inserting this into (41) yields the infimum

$$\inf_\mu F[\mu] = -\log Z[0] \equiv -W[0]. \tag{42}$$

Comparing with (36) this may be interpreted as the effective action for $J = \bar{L} = 0$. If we vary F in (41) keeping the expectation value of L fixed at $\bar{L}_{\boldsymbol{x}}$ by means of a Lagrange multiplier $J_{\boldsymbol{x}}$, we find the probability

$$p[L] = \frac{e^{-S+(J,L)}}{Z[J]}, \tag{43}$$

where J is to be viewed as a function of $\bar{L}$, obtained via inverting the implicit relation $\bar{L} = \delta W/\delta J$. Plugging (43) into (41) yields a new variational infimum which is precisely the effective action,

$$\inf_\mu\{F[\mu] | \langle L_{\boldsymbol{x}}\rangle_\mu = \bar{L}_{\boldsymbol{x}}\} = (J,\bar{L}) - W[J] \equiv \Gamma[\bar{L}]. \tag{44}$$

In the MF approximation for the effective action one minimizes only with respect to all *product measures* $\nu \in \mathcal{P}$,

$$d\nu[L] = \prod_{\boldsymbol{x}} d\nu_{ß\boldsymbol{x}}(L_{\boldsymbol{x}}), \qquad d\nu_{\boldsymbol{x}}(u) = p_{\boldsymbol{x}}(u) dh(u), \tag{45}$$

where h is the reduced Haar measure from (10). Hence, the exact expression (44) is replaced by its MF version according to

$$\inf_{\nu\in\mathcal{P}} (F[\nu] | \langle L_{\boldsymbol{x}}\rangle_\nu = \bar{L}_{\boldsymbol{x}}) \equiv U_{\mathrm{MF}}[\bar{L}]. \tag{46}$$

Clearly, from the variational principle, the MF effective action U_{MF} bounds the effective action Γ from above. Since the set of all product measures is not convex (unlike the set of all probability measures), the MF action need not be convex. We may, however, use its convex hull given by the double Legendre transformation, $\Gamma_{\mathrm{MF}} \equiv \mathfrak{L}^2(U_{MF})$, which for non−convex U_{MF} will be a better approximation, $\Gamma \le \Gamma_{\mathrm{MF}} \le U_{\mathrm{MF}}$.

For a product measure the entropy and mean action entering F in (46) turn into sums (of products) of single-site expectation values. With the abbreviation

$$\int d\nu_{\boldsymbol{x}}(u) f(u) \equiv \langle f\rangle_{\boldsymbol{x}}, \tag{47}$$

we find for the general class of character actions (28),

$$F[\nu] = \sum_{\langle \boldsymbol{xy}\rangle,(pq)} \lambda_{pq}\langle\chi_p\rangle_{\boldsymbol{x}}\langle\chi_q\rangle_{\boldsymbol{y}} + \sum_{\boldsymbol{x}} \langle \log p_{\boldsymbol{x}}\rangle_{\boldsymbol{x}}. \tag{48}$$

In order to find the extrema of this expression with respect to the measure $p_{\boldsymbol{x}}$ we have to introduce an external source $J_{p,\boldsymbol{x}}$ for every character $\chi_{p,\boldsymbol{x}}$. Again, these may be viewed as Lagrange multipliers fixing the expectation values $\langle\chi_p\rangle_{\boldsymbol{x}}$ at the mean fields $\bar{\chi}_{p,\boldsymbol{x}}$. As we are interested in the effective potential rather than the effective action we set all expectation values constant

$$\langle\chi_p\rangle_{\boldsymbol{x}} \equiv \langle\chi_p\rangle. \tag{49}$$

Then the single-site measures $\nu_{\boldsymbol{x}}$ are identical implying that the source is constant, $J_{p,\boldsymbol{x}} = j_p$. For what follows it is thus sufficient to consider densities or single-site expressions. With this in mind (48) becomes extremal for the (single-site) measure

$$p(u) = \frac{\exp\{-V(u) + \boldsymbol{j}\cdot\boldsymbol{\chi}(u)\}}{z(\boldsymbol{j})}, \tag{50}$$

where we have collected the sources $j_1, j_2, \ldots$ and characters $\chi_1, \chi_2, \ldots$ into vectors such that $\boldsymbol{j}\cdot\boldsymbol{\chi} = \sum j_p\chi_p$. Here V denotes the potential introduced in (33), and the normalization factor is the single-site partition function,

$$z(\boldsymbol{j}) \equiv \int dh(u) \exp\{-V(u) + \boldsymbol{j}\cdot\boldsymbol{\chi}(u)\}. \tag{51}$$

This measure replaces (43). In accordance with the discussion following (43) the components of $\boldsymbol{j}$ have to be eliminated from the single-site measure p. This is done by inverting the relations

$$\bar{\boldsymbol{\chi}}(\boldsymbol{j}) = \nabla_{\boldsymbol{j}} w(\boldsymbol{j}), \qquad w(\boldsymbol{j}) = \log z(\boldsymbol{j}), \tag{52}$$

which yields $\boldsymbol{j} = \boldsymbol{j}(\bar{\boldsymbol{\chi}})$. Since the Schwinger function $w(\boldsymbol{j})$ is strictly convex, this relation between the mean characters and sources is one-to-one. At this point it is convenient to introduce the convex Legendre transform γ of the Schwinger function,

$$\gamma(\bar{\boldsymbol{\chi}}) = \sup_{\boldsymbol{j}}\{\boldsymbol{j}\cdot\bar{\boldsymbol{\chi}} - w(\boldsymbol{j})\}. \tag{53}$$

It yields the inverse relation

$$\boldsymbol{j}(\bar{\boldsymbol{\chi}}) = \nabla_{\bar{\boldsymbol{\chi}}}\gamma(\bar{\boldsymbol{\chi}}). \tag{54}$$

For product measures and constant mean characters the infimum of (48) becomes the MF potential

$$u_{\mathrm{MF}}(\bar{\boldsymbol{\chi}}) = d\sum_{(pq)\neq 0}\lambda_{pq}\bar{\chi}_p\bar{\chi}_q + \gamma(\bar{\boldsymbol{\chi}}). \tag{55}$$

We mention in passing that u_{MF} bounds the exact effective potential from above and so does its convex hull,

$$\gamma_{\mathrm{MF}} = \mathfrak{Q}^2(u_{\mathrm{MF}}). \tag{56}$$

To make contact with the MF potential (46) depending solely on the order parameter $\bar{L}$ we use $\chi_1 = 2L$ and define the new MF potential (density)

$$u_{\mathrm{MF}}(\bar{L}) = \inf_{\bar{\chi}_2,\bar{\chi}_3,\ldots} u_{\mathrm{MF}}(2\bar{L}, \bar{\chi}_2, \bar{\chi}_3, \ldots). \tag{57}$$

Using results from [20] one can show that u_{MF} is the MF approximation to the *constraint effective potential* [21]. The formula (55) for the MF potential is still rather implicit as the expectation values $\langle\chi_p\rangle$ depend on the sources which have to be eliminated via (52).

To calculate the mean characters we only need the critical values of u_{MF}, and those are determined by the gap equations. Thus, to calculate the mean characters one may proceed as follows:

(1) Because of (54) the sources and mean characters at a critical point of $u_{\mathrm{MF}}(\bar{\boldsymbol{\chi}})$ are related as

$$j_p = -2d\sum_q \lambda_{pq}\bar{\chi}_q. \tag{58}$$

(2) We use these relations to eliminate the sources in the formula (55) for the mean characters, which read explicitly

$$\bar{\chi}_r = \frac{\int dh\,\chi_r(u)\exp\{\boldsymbol{j}\cdot\boldsymbol{\chi}(u) - V(u)\}}{\int dh\exp\{\boldsymbol{j}\cdot\boldsymbol{\chi}(u) - V(u)\}}, \tag{59}$$

with $dh = dh(u)$ from (10).

(3) These constitute a nonlinear transcendental system

$$\bar{\chi}_r = F_r(\bar{\boldsymbol{\chi}}), \tag{60}$$

with the right-hand side given explicitly by the integral expression

$$F_r = \frac{\int dh\,\chi_r(u)\exp\{-2d\sum\lambda_{pq}\bar{\chi}_q\chi_p(u) - V\}}{\int dh\exp\{-2d\sum\lambda_{pq}\bar{\chi}_q\chi_p(u) - V\}}. \tag{61}$$

which in principle yield $\bar{\boldsymbol{\chi}}$. In general, the solution of these gap equations can only be determined numerically. The gap Eqs. (60) are to be viewed as a system of nonlinear equations which determine the critical points $\bar{\chi}_p$ of u_{MF} as functions of the couplings λ_{pq}. This dependence approximates the true behavior of the vacuum expectation values $\langle\chi_p\rangle$.

B. Examples

In general the integrals (61) involved in the gap equations cannot be done analytically. Things become simple, however, if the PLA contains only two hopping terms as in (33),

$$T_2 = \sum_{\langle xy\rangle}(\lambda_{11}\chi_{1x}\chi_{1y} + \lambda_{22}\chi_{2x}\chi_{2y}). \tag{62}$$

In what follows we will concentrate on this particular case corresponding to NN interactions of Polyakov loops in the fundamental and adjoint representation, respectively. We are particularly interested in the behavior of the adjoint loop χ_2. This is center symmetric by itself and hence, strictly speaking, does not constitute an order parameter. On the other hand, if the symmetric phase is dominated by the Haar measure (corresponding to equipartition, i.e. $S_{pq} \simeq 0$) *all* nontrivial characters have vanishing expectation value due to orthogonality. In the broken phase, the higher characters may then develop expectation values driven by the fundamental loop and serve as approximate order parameters. For gauge group $SU(3)$ this was observed recently in [15].

For the effective action T_2 the gap Eqs. (60) are

$$\bar{\chi}_1 = F_1(\bar{\chi}_1, \bar{\chi}_2, \lambda_{11}, \lambda_{22}), \tag{63}$$

$$\bar{\chi}_2 = F_2(\bar{\chi}_1, \bar{\chi}_2, \lambda_{11}, \lambda_{22}). \tag{64}$$

In the symmetric phase ($\bar{L} = 0$) and close to the phase transition we may linearize (63) and (64) to leading order around $\bar{\chi}_1 = 0$,

$$\bar{\chi}_1 \simeq \bar{\chi}_1\frac{\partial}{\partial\bar{\chi}_1}F_1(\bar{\chi}_1, \bar{\chi}_2)\Big|_{\bar{\chi}_1=0}, \tag{65}$$

$$\bar{\chi}_2 \simeq F_2(0, \bar{\chi}_2). \tag{66}$$

Discarding the trivial solution $\bar{\chi}_1 = 0$ and evaluating the integrals $F_{1,2}$ the gap Eqs. (65) and (66) become

$$1 = -2d\lambda_{11}(1 + F_2(0, \bar{\chi}_2)), \tag{67}$$

$$\bar{\chi}_2 = F_2(0, \bar{\chi}_2), \tag{68}$$

with

$$F_2(0, \bar{\chi}_2) = \frac{I_1(j) - 2d\lambda_{22}\bar{\chi}_2[I_0(j) + I_1(j)]}{2d\lambda_{22}\bar{\chi}_2[I_0(j) + I_1(j)]}, \tag{69}$$

and $j \equiv 4d\lambda_{22}\bar{\chi}_2$ being the argument of the modified Bessel functions I_0, I_1. The result (69) shows that (66) is independent of the coupling λ_{11} and thus determines $\bar{\chi}_2(\lambda_{22})$ near $\bar{\chi}_1 = 0$. The numerical solution yields the

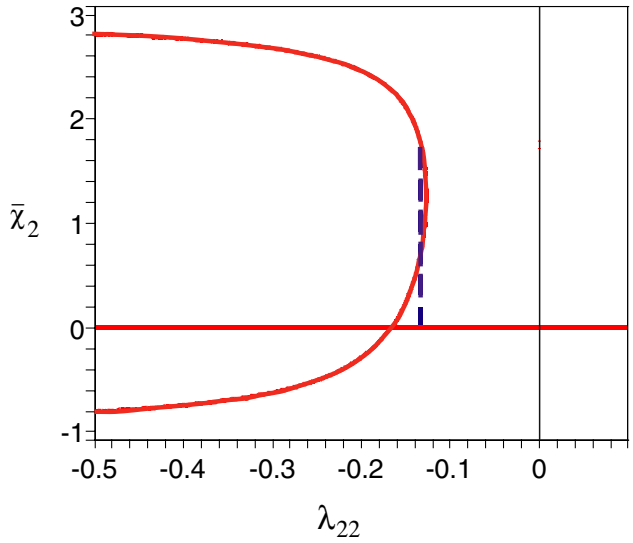

FIG. 2 (color online). Expectation value of the adjoint mean Polyakov loop $\bar{\chi}_2$ as a function of the coupling λ_{22} near the phase transition in λ_{11}. The dashed line represents the "first-order" jump from $\bar{\chi}_2 = 1.671$ to zero at $\lambda_{22c} = -0.133$. The bifurcation point is located at $\lambda_{22} = -0.167$ while for $\lambda_{22} > -0.127$ there is only the trivial solution $\bar{\chi}_2 = 0$.

typical bifurcation behavior shown in Fig. 2. For $\lambda_{22} < -0.127$ there are generically three solutions for $\bar{\chi}_2(\lambda_{22})$, the trivial one, $\bar{\chi}_2 = 0$, and two nontrivial ones.

Obviously, we still have to determine which solution corresponds to the absolute minimum of the MF potential as a function of $\bar{\chi}_2$. To proceed analytically, we approximate the latter by simply integrating the gap Eqs. (63) and (64) with respect to the characters. This results in the approximate MF potential

$$u(\bar{\chi}_1, \bar{\chi}_2, \lambda_{11}, \lambda_{22}) \equiv -d \sum_{p=1,2} \lambda_{pp} \bar{\chi}_p^2 - w(\bar{\chi}_1, \bar{\chi}_2, \lambda_{11}, \lambda_{22}), \tag{70}$$

which coincides with the MF potential at the critical points. For $\bar{\chi}_1 = 0$ the relevant integrals can be done analytically and again lead to modified Bessel functions. One finds that the absolute minimum of $u(0, \bar{\chi}_2, 0, \lambda_{22})$ is located at $\bar{\chi}_2 > 0$ for sufficiently negative values of λ_{22}. At the "critical" value $\lambda_{22} = -0.133$ its locus suddenly jumps from $\bar{\chi}_2 = 1.671$ to $\bar{\chi}_2 = 0$ (the dashed line in Fig. 2) where it stays for λ_{22} growing larger.

Combining (65) and (66) yields the critical coupling λ_{11c} as a function of $\bar{\chi}_2(\lambda_{22})$,

$$\lambda_{11c} = -\frac{1}{2d(1 + \bar{\chi}_2)}. \tag{71}$$

For the trivial solution, $\bar{\chi}_2 = 0$, we find the universal critical coupling

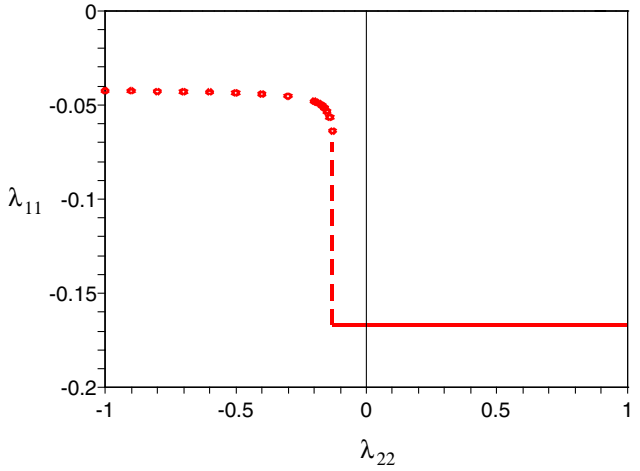

FIG. 3 (color online). Critical line $\lambda_{11}(\lambda_{22})$ corresponding to the phase boundary at which $\bar{L} = \bar{\chi}_1/2$ develops a nonvanishing expectation value. The sudden "drop" at $\lambda_{22} = -0.133$ (dashed line) is due to the "first-order behavior" of $\bar{\chi}_2$ displayed in Fig. 2.

$$\lambda_{11c} = -\frac{1}{2d}, \tag{72}$$

which only depends on the dimension d.

Plugging the numerical solution $\bar{\chi}_2(\lambda_{22})$ from Fig. 2 corresponding to the absolute minimum of the MF potential into (71) we finally obtain the critical line in the plane of couplings λ_{11} and λ_{22} displayed in Fig. 3. The discontinuity in $\bar{\chi}_2$ translates into the sudden drop of λ_{11} at $\lambda_{22} = -0.133$.

We have checked the results above by calculating the behavior of the character expectation values numerically without using the approximations (65) and (66) to eliminate the sources. The results for $\bar{L} = \bar{\chi}_1/2$ and $\bar{\chi}_2$ as a function of the couplings are shown in Figs. 4 and 5.

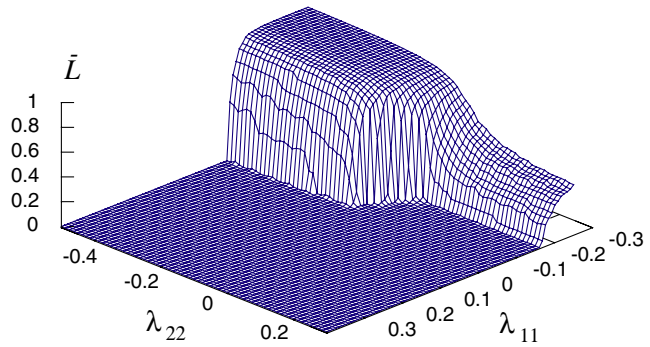

FIG. 4 (color online). The order parameter $\bar{L} = \bar{\chi}_1/2$ for the Ising-type PLA T_2 from (65). Off the critical region around $\lambda_{22} = -0.133$ the phase boundary agrees perfectly well with the critical line of Fig. 3.

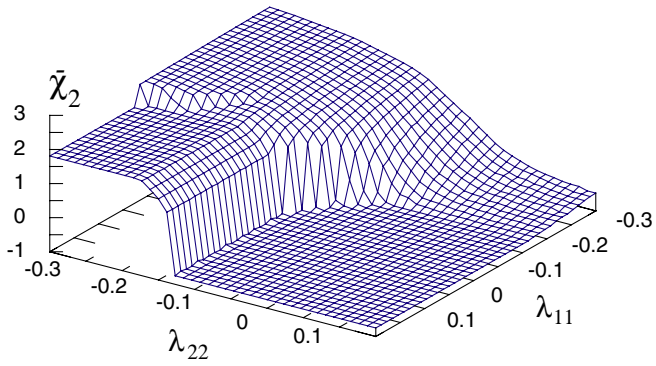

FIG. 5 (color online). Numerically exact MF behavior of the adjoint Polyakov loop $\bar{\chi}_2$ for the PLA T_2 from (62).

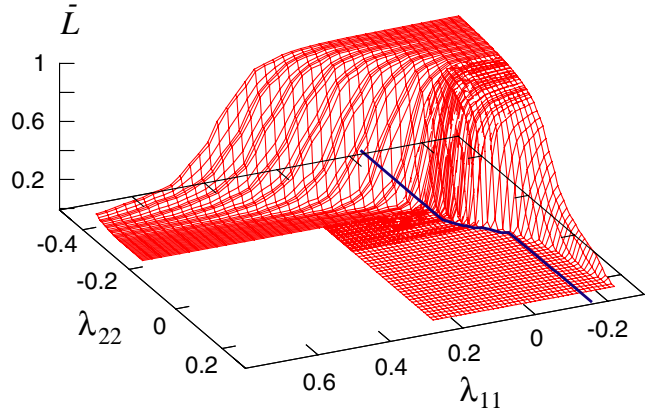

FIG. 6 (color online). MC data showing the order parameter $\bar{L}$ for the Ising-type PLA T_2 from (62). The dark curve represents the critical line (phase boundary) from Fig. 4.

Most notable are the following features. First, the critical line of Fig. 3 approximates the phase boundary of Fig. 4 very well (except for the neighborhood of the critical value $\lambda_{22c} \simeq -0.133$). Second, for $\lambda_{22} < \lambda_{22c}$ there is indeed a first–order phase transition at $\lambda_{11} \simeq -0.04$ where $\bar{L}$ suddenly jumps to a finite value.

To assess the quality of the MF approximation we have performed a direct MC simulation of the PLA (62). In Fig. 6 we have plotted the MC results for the order parameter $\bar{L}$ as a function of the couplings. Shown is $\bar{L}$ for several thousand sample points in the $(\lambda_{11}, \lambda_{22})$ plane. Near the phase boundary about 2.5 M updates were sufficient for $\lambda_{22} \gtrsim -0.1$, whereas for $\lambda_{22} \lesssim -0.1$ at least 50 M updates were required. We interpret this slow convergence as a signal for a first-order phase transition as predicted by the MF approximation, see Fig. 4. The continuous behavior across the phase boundary for $\lambda_{22} \lesssim -0.1$ thus presumably represents a hysteresis effect. With our local MC algorithm we have not been able to check this in detail.

Resuming thus far it seems fair to say that the phase structure of the PLAs becomes quite involved if more than just one character (i.e. Polyakov loops in higher representations) are included.

In order to make contact with known results we conclude this subsection with a few remarks on the simplest PLA with only one character. This is straightforwardly obtained from (62) by setting $\lambda_{22} = 0$,

$$S_1 \equiv T_1 = \sum_{\langle xy \rangle} \lambda_{11} \chi_{1x} \chi_{1y}. \tag{73}$$

Note that our sign-convention is such that *negative* λ_{11} corresponds to "ferromagnetism." The Ising-type model (73) has first been studied by Polónyi and Szlachányi [22] who also derived it using a strong-coupling expansion. According to (72) the MF critical coupling is $\lambda_{11c} = -1/2d$ locating a second-order phase transition. The MF potential of the model (73) is

$$u_{\mathrm{MF}}(\ell) = 4d\lambda_{11}\ell^2 + \ell j - w_0(j), \tag{74}$$

where the relation $2\ell = \partial w_0/\partial j$ has to be inverted to trade the source j for the Polyakov loop ℓ via $j = j(\ell)$. This potential is minimal for $\ell = \bar{L}$ which solves

$$j(\bar{L}) = -8d\lambda_{11}\bar{L}, \tag{75}$$

implying the self-consistency condition

$$2\bar{L} = (-8d\lambda_{11}\bar{L})\frac{I_1(j) - I_3(j)}{I_0(j) - I_2(j)}, \tag{76}$$

with the argument $j = j(\bar{L})$ from (75). The effective potential and order parameter are plotted in Fig. 7. Near the critical coupling the order parameter has the typical square

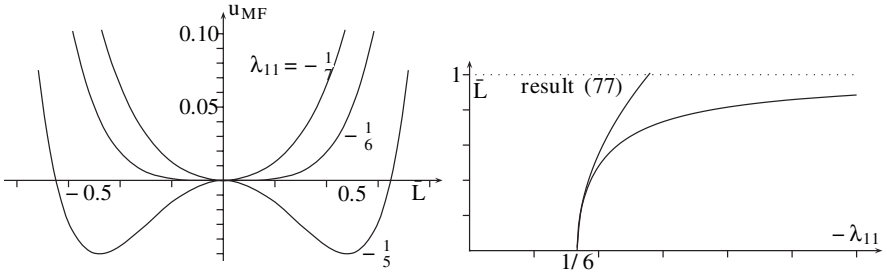

FIG. 7. MF prediction for the effective potential and order parameter for the Ising-type PLA $S_1 = T_1$ from (73).

root behavior,

$$\bar{L} \approx \sqrt{\frac{3}{2}}\sqrt{\frac{\lambda_{11}}{\lambda_{11c}} - 1} \quad \text{for} \quad |\lambda_{11}| \searrow |\lambda_{11c}|, \tag{77}$$

which is also displayed in Fig. 7.

V. IMC RESULTS FOR $\lambda_{pq}(\beta)$

Employing our IMC method based on the geometrical Schwinger-Dyson equations of Sec. II we have calculated the couplings λ_{pq} for different PLAs as functions of β (see [23,24] for earlier IMC results in a similar context). For our lattice with $N_s = 20$ and $N_t = 4$ (the maximum value we can achieve with our computer resources) the critical Wilson coupling is $\beta_c = 2.30$. Below β_c we find the hierarchy

$$|\lambda_{11}| \gg |\lambda_{22}|, \qquad |\lambda_{02}| \gg |\lambda_{33}|, \qquad |\lambda_{13}|, \tag{78}$$

in agreement with the *strong-coupling* expansion (24)–(26). According to Ogilvie [25], the *weak-coupling* asymptotics of λ_{11} is linear in β,

$$\lambda_{11}(\beta) = -\frac{\beta}{2N_C N_t} + \text{const.} \qquad (\beta \gg \beta_c),$$

which in our case ($N_C = 2$) leads to

$$\lambda_{11}(\beta) = -\frac{\beta}{16} + \text{const.} = -0.0625\beta + \text{const.} \tag{79}$$

We have compared our IMC results for the couplings $\lambda_{pq}(\beta)$ with the strong-coupling predictions (17) and (27)–(30), and the weak-coupling result (79). As expected from our reasoning above, the lowest order PLAs based on group characters approximate the true Polyakov-loop dynamics very well in the *strong-coupling* regime. For weak coupling we find the linear relation (79) already for the LO PLA. For the NLO Ginzburg-Landau-type model with 3 couplings the slope -0.0614 is very close to the weak-coupling result -0.0625 in (79). Thus we are confident that our PLAs describe the true Polyakov-loop dynamics *below and above* the critical Wilson coupling very well.

A. Leading-order action

The effective couplings λ_{11} for the LO Ising-type model (73) for β-values below and above the critical $\beta_c = 2.30$ are listed in Table VI, Appendix A. We read off the value $\lambda_{11}(\beta_c) = -0.132$. If S_1 would be the exact PLA then its critical coupling λ_{11c} would be $\lambda_{11}(\beta_c)$. A direct MC simulation of the action S_1 reveals that this model has critical coupling $\lambda_{11c} = -0.18$. The MF prediction $\lambda_{11c} = -0.17$ comes surprisingly close to the former "true" value. The critical coupling may alternatively be estimated by using the strong-coupling results (18) and (24) to calculate $\lambda_{11}(\beta_c)$ (extrapolating them to $N_t = 4$ and $\beta_c = 2.30$),

$$\lambda_{11} = -(\beta/4)^{N_t} \overset{\beta=\beta_c}{\approx} -0.11. \tag{80}$$

TABLE I. Comparison of the critical coupling values for the LO Ising-type model S_1. The "exact" value is obtained via MC simulation.

Method	Critical coupling
MC simulation	$\lambda_{11c} = -0.18$
MF	$\lambda_{11c} = -0.17$
Strong coupling	$\lambda_{11c} = -0.11$
IMC	$\lambda_{11}(\beta_c) = -0.14$

The output of the different methods is compiled in Table I. The values obtained are quite close to each other. The true value -0.18 stems from simulating (73) with the MF approximation coming closest. Somewhat surprisingly, the strong-coupling result yields the right order of magnitude. The discrepancy between direct simulation and IMC just means that the action (73) represents an oversimplification and does not match with Yang-Mills well enough. The IMC value $\lambda_{11}(\beta_c) = -0.14$ constitutes a compromise equivalent to a one-parameter fit of the effective to the Yang-Mills Schwinger-Dyson equations or n-point functions.

In Fig. 8 we compare the results for λ_{11} from strong- and weak-coupling expansion with the data of our IMC simulations. Note that the asymptotic formula (83) works up to $\beta \simeq 2$. The IMC values for the LO action S_1 in (76) are marked with circles. Note further that the dependence $\lambda_{11}(\beta)$ is indeed linear in the weak-coupling regime,

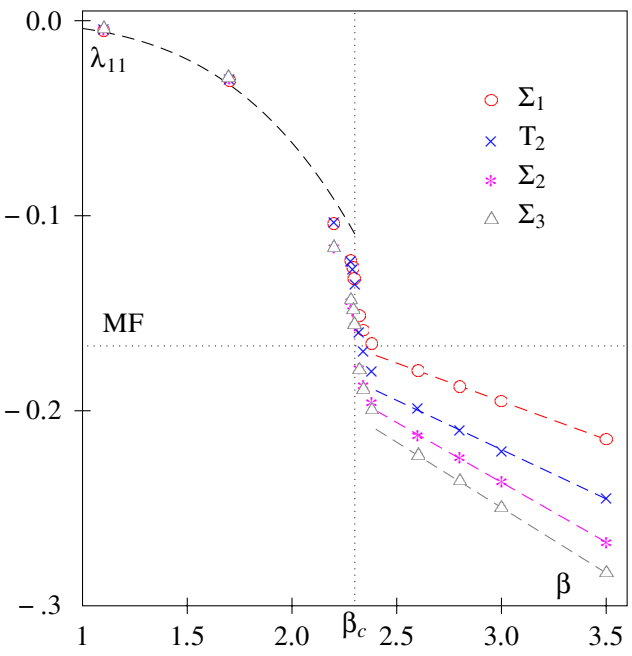

FIG. 8 (color online). The coupling λ_{11} as a function of β. Dashed curve for $\beta < \beta_c$: asymptotic behavior (80); dashed lines for $\beta > \beta_c$: linear fits $\lambda = a\beta + b$; data points: IMC results from Tables VI, VII, and VIII in Appendix A.

$\lambda_{11} = -0.0392\beta - 0.0774$, in accordance with the prediction (82) for the weak-coupling asymptotics. The slope, however, turns out being too small. This will be remedied in what follows by including more couplings.

B. Next-to-leading-order actions

The effective action (73) has been confirmed and extended by several authors [23–28]. We have also checked its generalizations by considering the NLO Ising-type model (62) without potential terms and the "Ginzburg-Landau action" (33) containing all NLO terms including the potential V_2.

The NLO IMC results for $\lambda_{11}(\beta)$ are displayed in Fig. 8 (crosses and asterisks), those for $\lambda_{22}(\beta)$ in Fig. 9 (same symbols) and those for $\lambda_{02}(\beta)$ in Fig. 10 (asterisks). The error bars for the couplings are listed in the tables in Appendix A. Upon comparing the values for λ_{11} in Fig. 8 (or Table VI) we note that for $\beta < \beta_c$ the predictions for λ_{11} are almost model independent. In the weak-coupling regime, on the other hand, they are less stable. Hence, adding terms to the PLA may change the coupling constants considerably in this regime.

For the NLO actions the dependence $\lambda_{11}(\beta)$ is linear in the weak-coupling regime, similarly as for the LO action S_1. However, the slopes a in the linear fits $\lambda_{11}(\beta) = a\beta + b$ above β_c are model dependent. For the LO and NLO PLA they are given in Table II together with the weak-coupling result (79). For the Ising-type models without potential terms the slope is not reproduced very well, and we conclude that in the weak-coupling or high-temperature regime potential terms should be included for an accurate description of the Polyakov-loop dynamics. Indeed, the slope for the action (33) with potential term V_2 is almost identical to the prediction (79) of the weak-coupling asymptotics.

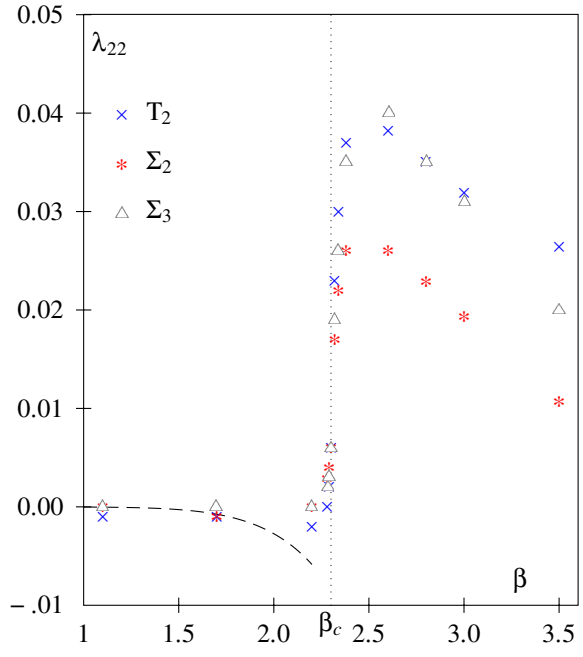

FIG. 9 (color online). The adjoint coupling λ_{22} as a function of β for the NLO and NNLO actions. Dashed curve: asymptotic behavior (81); data points: IMC results from Tables VI, VII, and VIII.

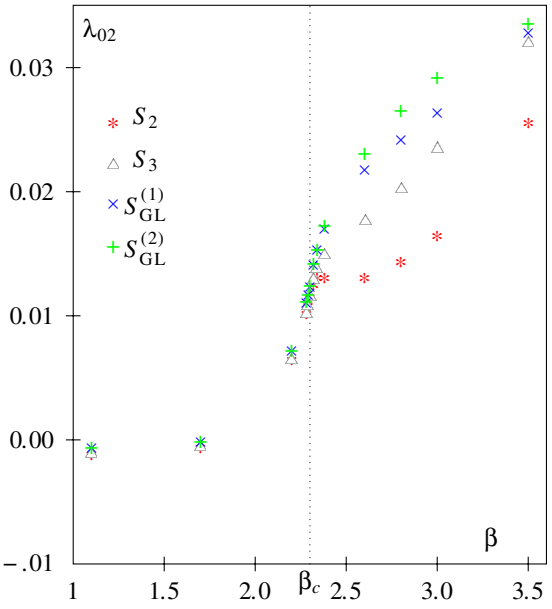

FIG. 10 (color online). The coupling λ_{02} as a function of the Wilson coupling β for NLO, NNLO and Ginzburg-Landau actions; data points: IMC results from Tables VII, VIII, and IX.

Figure 9 shows the dependence of the adjoint coupling constant λ_{22} on the Wilson coupling β. Also shown is the prediction (25) of the strong-coupling expansion using (18),

$$\lambda_{22}(\beta) = -\frac{113}{162}\left(\frac{\beta}{4}\right)^8 \approx -0.69753\left(\frac{\beta}{4}\right)^8, \qquad (81)$$

which again reproduces the IMC results for $\beta < 2$.

The critical coupling

$$\lambda_{22}(\beta_c) = 0.006[1] \qquad (82)$$

is the same for both PLAs (62) and (33), hence independent of V_2. Up to β_c the two actions have almost identical couplings λ_{22}. It seems that for $\beta > \beta_c$ these couplings also depend linearly on β, as was the case for $\lambda_{11}(\beta)$. The positive value for λ_{22} (for $\beta\beta_c$) is consistent with earlier results [29].

TABLE II. Slopes of the linear fits to the weak-coupling asymptotics (79) of λ_{11}.

Model	$1/2N_CN_t$	S_1	T_2	S_2
Slope	−0.0625	−0.0392	−0.0505	−0.0614

C. Next-to-next-to-leading order

We have seen that the NLO approximations describe the Polyakov-loop dynamics very well in the symmetric strong-coupling phase. In the weak-coupling regime, however, there is still room for improvement. Hence we have calculated the five coupling constants λ_{11}, λ_{22}, λ_{02}, λ_{13}, λ_{33} appearing in the general NNLO PLA S_3 for several values of the Wilson coupling. This action is the sum of all terms up to order $\beta_t^{3N_t}$ in the strong-coupling expansion. As expected, adding the third order terms S_{31} and S_{33} does not change the lower−order couplings λ_{11}, λ_{22}, λ_{02} (as obtained via S_2) in the broken phase. This can be seen in Figs. 8–10, where the IMC results for the NNLO action S_3 from (34) are depicted by triangles. The numerical values for these couplings and the couplings λ_{33} and λ_{13} together with their statistical errors are given in Appendix A.

D. Ginzburg-Landau models

In his review [9], Svetitsky has suggested to emphasize the potential term in (3) by specializing to an ansatz of Ginzburg-Landau type,

$$S_{\mathrm{GL}} = S_1 + \sum_{\boldsymbol{x}} V(L_{\boldsymbol{x}}), \tag{83}$$

with center-symmetric potential (30). Replacing the coefficients λ_{0p} of the characters in this potential by

$$\lambda_4 = 2d \cdot 4^2 \lambda_{04}, \tag{84}$$

$$\lambda_2 = 2d \cdot 4(\lambda_{02} - 3\lambda_{04}), \tag{85}$$

leads for $p \leq 4$ to the even polynomial

$$V(L) = \lambda_2 L^2 + \lambda_4 L^4 + \text{const.} \tag{86}$$

In Table IX we have listed the couplings for the models with quadratic and quartic potentials,

$$S_{\mathrm{GL}}^{(1)} = S_1 + \lambda_2 \sum_{\boldsymbol{x}} L_{\boldsymbol{x}}^2, \tag{87}$$

$$S_{\mathrm{GL}}^{(2)} = S_{\mathrm{GL}}^{(1)} + \lambda_4 \sum_{\boldsymbol{x}} L_{\boldsymbol{x}}^4, \tag{88}$$

obtained via IMC within our standard range of β. The values for λ_{11} both for strong and weak coupling are almost identical to those of the NLO model S_2. For this reason we have refrained from plotting them in Fig. 8. The potential couplings are important in the broken weak-coupling phase where they become sizable. The coupling λ_{02} for the Ginzburg-Landau models (87) and (88) is shown in Fig. 10.

E. Summary

The values for the couplings of the different PLAs arising at critical Wilson coupling $\beta_c = 2.30$ are listed in Table III. They are almost model independent. λ_{11}, in particular, is always close to the MF value -0.167 (for the Ising-type models).

TABLE III. Effective couplings of different PLAs at $\beta = \beta_c = 2.30$.

Model	S_1	T_2	S_2	S_3	$S_{\mathrm{GL}}^{(2)}$
$\lambda_{11}(\beta_c)$	−0.133	−0.135	−0.156	−0.156	−0.155
$\lambda_{22}(\beta_c)$		0.006	0.006	0.006	
$\lambda_{02}(\beta_c)$			0.011	0.012	0.012

The couplings below and above β_c and their statistical errors are compiled in Appendix A. There one may also find λ_{33}, λ_{13} and $\lambda_{04} = \lambda_4/32d$ for different Wilson couplings.

The stability of the couplings for $\beta < \beta_c$ is a strong indication that (in this regime) the Yang-Mills ensemble is very well approximated already by the NLO models with 2 or 3 couplings. The results of the following section will further confirm this statement.

The Ising-type coupling λ_{11} becomes a linear function of β in the weak-coupling regime, in accordance with the weak-coupling prediction (79). For the NLO action the slope is -0.0614 which compares favorably with the weak−coupling value -0.0625. For the Ginzburg-Landau-type actions the slope is almost identical to the one of the NLO models.

The Ising-type couplings change rapidly at the critical Wilson coupling $\beta_c = 2.30$ as demonstrated in Figs. 8 and 9. For example, the coupling λ_{11} decreases from -0.1 below β_c to -0.2 above β_c. This jump of λ_{11} forces the system into the ferromagnetic phase. For λ_{22} the jump is even more dramatic, from 0 to 0.04. The potential couplings λ_{02} and λ_{04} change more smoothly when the systems changes from the symmetric to the broken phase.

VI. TWO-POINT FUNCTIONS

Let us finally check the quality of our PLAs which, after all, should represent approximations to Yang-Mills theory. To this end we compare the Yang-Mills two-point function at different β-values with those of our effective models inserting the couplings $\lambda_{pq}(\beta)$ obtained via IMC. For the NLO actions at $\beta = 2.2$ these couplings are displayed in Table IV, while for $\beta = 3.0$ we have the NLO and NNLO couplings of Table V. With these couplings we have simulated the models with actions

$$T_2, \quad S_2, \quad S_3, \quad S_{\mathrm{GL}}^{(1)}, \quad S_{\mathrm{GL}}^{(2)}, \tag{89}$$

and calculated the two-point functions displayed in

TABLE IV. Effective couplings for NLO actions at $\beta = 2.2$.

$\beta = 2.2$	λ_{11}	λ_{22}	λ_{20}
T_2	0.1033	0.0019	
S_2	0.1168	0.00042	0.0064

TABLE V. Effective couplings for NLO and NNLO actions at $\beta = 3.0$.

$\beta = 3$	λ_{11}	λ_{22}	λ_{20}	λ_{33}	λ_{31}
T_2	0.2207	0.0320			
S_2	0.2361	0.0194	0.0165		
S_3	0.2506	0.0311	0.0236	0.0035	0.0040

Figs. 11 and 12. As expected, the agreement in the center-symmetric phase ($\beta = 2.2$) is very good, while deep in the broken phase ($\beta = 3.0$) there appears to be room for improvement. For $\beta = 2.2$ the two-point functions of the three effective models considered are almost identical to the Yang-Mills two-point function. The data points for S_3 and $S^{(2)}_{\mathrm{GL}}$ cannot be distinguished from those for the NLO model S_2 and hence are not displayed in Fig. 11.

For $\beta = 3.0$ the two-point functions and the expectation value of the mean field are model dependent. In Fig. 12 we have plotted the two-point function of Yang-Mills theory and of the NLO and NNLO effective actions.

For the NLO approximation T_2 the value for the condensate is approximately 20% below the Yang-Mills value. Including potential terms (S_2) and NNLO terms (S_3) improves the approximation somewhat as Fig. 12 shows. The two-point function for the Ginzburg-Landau action $S^{(2)}_{\mathrm{GL}}$ is almost identical to the one of T_2 (and thus has not been displayed). This implies that also higher-order Ising (or hopping) terms are important when $\beta > \beta_c$.

VII. DISCUSSION

To really obtain satisfactory approximations to Yang-Mills expectation values (e.g. two-point functions) for all

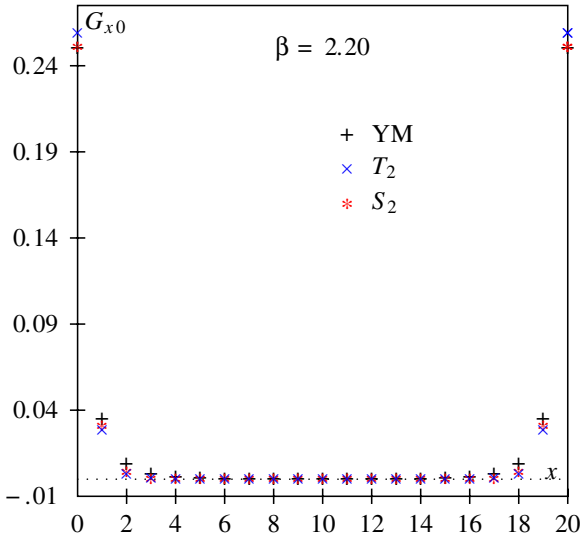

FIG. 11 (color online). The Yang-Mills (YM) two-point function compared to the ones obtained from the NLO effective actions T_2 and S_2; $(N_s, N_t) = (20, 4)$.

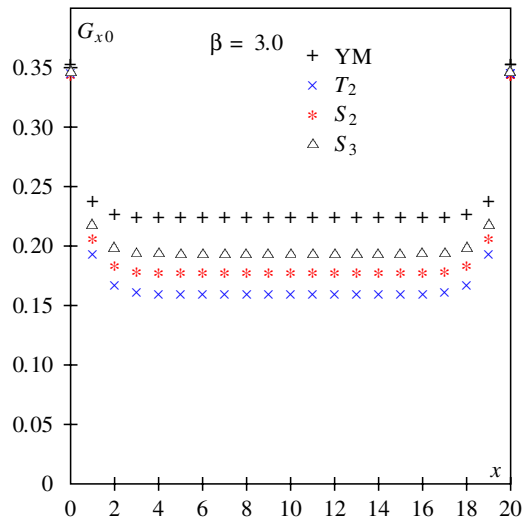

FIG. 12 (color online). The Yang-Mills (YM) two-point function compared to the one obtained from the NLO (T_2 and S_2) and NNLO (S_3) effective actions; $(N_s, N_t) = (20, 4)$.

β-values one has to go beyond nearest-neighbor interactions in the effective theory. This has been done in [16] where operators with $r \equiv |\boldsymbol{x} - \boldsymbol{y}|$ up to $\sqrt{2}$ ("plaquette operators") were included. We briefly recapitulate the results of this brute-force calculation. By reformulating the Schwinger-Dyson equations (12) in terms of characters, the couplings have been determined by our standard inverse Monte Carlo routines. We found that the couplings decrease rapidly not only if we go to higher representations (i.e. larger p) as above, but also if we increase the number of links within the plaquette operators used. The leading $r = 1$ term S_1 of (32) with coupling λ_{11} dominates by 1 order of magnitude compared to the terms with $r = \sqrt{2}$. This clearly indicates that the effective interactions are short ranged in accordance with the Svetitsky-Yaffe conjecture. Simulating the effective action including plaquette operators with the couplings obtained via IMC we have calculated the two-point function in both phases. Including a total of 14 couplings the matching between Yang-Mills and the effective action becomes perfect both in the broken and symmetric phase [16]. It should, however, be stressed that this brute-force numerical calculation does not provide too much of physical intuition. We believe that the present paper, in particular, the mean-field analysis, improves upon [16] in this respect.

The most straightforward generalization of our analysis obviously is to go to $SU(3)$ Yang-Mills theory where one expects a first-order phase transition. Work in this direction is under way.

ACKNOWLEDGMENTS

We thank L. Dittmann for his collaboration at an early stage of this work and A. Dumitru for useful discussions.

Special thanks go to B. Pozsgay for pointing out a flaw in our earlier mean-field calculations. T. H. is indebted to A. Hart, R. Pisarski, and A. Khvedelidze for sharing valuable insights. T. K. acknowledges useful hints from A. Sternbeck and D. Peschka.

APPENDIX A: TABLES

The following Tables VI, VII, VIII, and IX contain the effective couplings λ_{pq} with statistical errors for various values of β.

TABLE VI. IMC results for the effective coupling λ_{11} in the LO action S_1 and the two couplings λ_{11}, λ_{22} in T_2.

Yang-Mills-β	S_1:λ_{11}	T_2:λ_{11}	T_2:λ_{22}
1.70	−0.0305[4]	−0.030[2]	−0.001[1]
2.20	−0.1040[2]	−0.103[1]	−0.0019[7]
2.28	−0.1231[3]	−0.123[1]	0.000[1]
2.29	−0.1267[4]	−0.127[1]	0.002[1]
2.30	−0.1325[5]	0.135[1]	0.006[1]
2.32	−0.1512[3]	−0.1598[9]	0.023[1]
2.34	−0.1585[2]	−0.1697[6]	0.030[1]
2.38	−0.1658[1]	−0.1799[4]	0.037[1]
2.60	−0.1792[1]	−0.1989[4]	0.0382[8]
2.80	−0.1874[1]	−0.2103[5]	0.0350[8]
3.00	−0.1952[1]	−0.2206[6]	0.0319[8]
3.50	−0.2146[1]	−0.2446[6]	0.0264[6]
4.00	−0.2343[1]	−0.2670[9]	0.0225[6]

TABLE VII. IMC results for the three couplings in S_2.

β	λ_{11}	λ_{22}	λ_{20}
1.10	−0.004[4]	−0.000[2]	−0.0012[5]
1.70	−0.030[4]	−0.001[2]	−0.0007[5]
2.20	−0.116[2]	0.000[2]	0.0064[5]
2.28	−0.144[2]	0.002[2]	0.0101[5]
2.29	−0.148[2]	0.004[2]	0.0108[5]
2.30	−0.156[2]	0.006[2]	0.0114[5]
2.32	−0.178[2]	0.017[2]	0.0125[6]
2.34	−0.187[1]	0.022[2]	0.0130[6]
2.38	−0.195[1]	0.026[2]	0.0130[6]
2.60	−0.212[1]	0.026[2]	0.013[1]
2.80	−0.224[1]	0.022[2]	0.014[1]
3.00	−0.236[1]	0.019[2]	0.016[1]
3.50	−0.267[1]	0.010[2]	0.025[1]
4.00	−0.299[1]	0.003[2]	0.037[1]

TABLE VIII. IMC results for five couplings in S_3.

β	λ_{11}	λ_{22}	λ_{20}	λ_{33}	λ_{31}
1.10	−0.004[1]	0.000[1]	−0.0011[2]	0.000[1]	0.0003[6]
1.70	−0.029[2]	0.000[1]	−0.0006[2]	0.0001[8]	0.0000[6]
2.20	−0.116[1]	0.000[1]	0.0064[2]	0.0015[7]	0.0000[6]
2.28	−0.143[1]	0.002[1]	0.0102[3]	0.0015[8]	0.0002[6]
2.29	−0.148[1]	0.003[1]	0.0108[3]	0.0015[8]	0.0000[6]
2.30	−0.156[1]	0.006[1]	0.0115[3]	0.001[1]	0.0000[6]
2.32	−0.179[1]	0.019[1]	0.0129[3]	−0.0006[9]	−0.0004[5]
2.34	−0.1892[8]	0.026[1]	0.0138[3]	−0.0014[8]	−0.0014[6]
2.38	−0.1999[6]	0.035[1]	0.0148[4]	−0.0032[9]	−0.0026[5]
2.60	−0.2227[8]	0.040[1]	0.0176[5]	−0.005[1]	−0.0041[4]
2.80	−0.236[1]	0.035[1]	0.0202[8]	−0.0041[9]	−0.0040[4]
3.00	−0.250[1]	0.031[1]	0.0235[8]	−0.0034[8]	−0.0039[4]
3.50	−0.283[1]	0.020[1]	0.032[1]	−0.002[1]	−0.0032[6]
4.00	−0.291[3]	0.003[1]	0.029[2]	−0.0033[9]	0.0029[8]

TABLE IX. IMC results for the couplings λ_{11}, λ_2, λ_4 in $S^{(2)}_{\mathrm{GL}}$.

β	λ_{11}	λ_2	λ_4
2.20	−0.110	0.186	−0.002
2.25	−0.119	0.237	−0.003
2.28	−0.127	0.288	−0.006
2.29	−0.128	0.303	−0.007
2.30	−0.157	0.453	−0.020
2.32	−0.173	0.621	−0.057
2.34	−0.176	0.698	−0.093
2.40	−0.190	0.979	−0.256

APPENDIX B: NUMERICAL DETAILS

All MC calculations have been performed on a $20^3 \times 4$ lattice for which the critical Wilson coupling is $\beta_c = 2.30$. The simulations have been done for β ranging from 1.1 to 4.0. We have used a standard ''pseudoheatbath'' algorithm [30,31] due to Miller [32].

The IMC routine has been implemented as follows. For each action term S_{pq} and site we have chosen the operator

$$G_{pq,z} \equiv \frac{1}{\lambda_{pq}} \frac{\delta S_{pq}}{\delta L_z}, \tag{B1}$$

which leads to the Schwinger-Dyson equations

$$\sum_{(pq)} \lambda_{pq} \langle (1 - L_x^2) G_{pq,z} S_{pq,x} \rangle = \langle (1 - L_x^2) G_{,x} - 3 L_x G \rangle. \tag{B2}$$

Because of translational invariance the coefficients of G_z and $G_{z'}$ are equal if $|x - z| = |x - z'|$. In order to have a sufficiently overdetermined system (for fixed pq) we choose the N_s operators $G_{pq,d}$, $d = 0 \ldots N_s$. Independent of our choice of PLA we have always used the full set of operators up to truncation values $p, q = 5$, i.e.

$$G_{11},\ G_{22},\ G_{20},\ G_{33},\ G_{31},\ G_{44},\ G_{42},\ G_{40},\ G_{55} \tag{B3}$$

with $0 \leq d \leq 8$ leading to a total of 81 operators (and equations). Translational invariance admits to use the spatial average of each Schwinger-Dyson equation and every configuration. The overdetermined system is then solved via least-square methods. We have checked that the couplings obtained in this way follow a normal distribution, as expected. Hence we calculated the standard deviation σ and took 2σ as our error. Autocorrelation effects have been eliminated via binning. Our statistics (5 k to 10 k configurations) entail a statistical error of 10^{-4} which translates into an uncertainty for the couplings in the NLO action of the order of a few percent. The NNLO couplings λ_{33} and λ_{31}, however, have statistical errors of about 20%.

Systematic errors are mainly due to the dependence of the couplings on the operator bases used in the Schwinger-Dyson equations.

[1] A. M. Polyakov, Phys. Lett. B **72**, 477 (1978).
[2] L. Susskind, Phys. Rev. D **20**, 2610 (1979).
[3] M. Caselle and M. Hasenbusch, Nucl. Phys. **B470**, 435 (1996).
[4] F. Gliozzi and P. Provero, Phys. Rev. D **56**, 1131 (1997).
[5] P. de Forcrand and L. von Smekal, Phys. Rev. D **66**, 011504 (2002).
[6] M. Pepe and P. de Forcrand, Nucl. Phys. B Proc. Suppl. **106**, 914 (2002).
[7] B. Svetitsky and L. Yaffe, Nucl. Phys. **B210**, 423 (1982).
[8] L. G. Yaffe and B. Svetitsky, Phys. Rev. D **26**, 963 (1982).
[9] B. Svetitsky, Phys. Rep. **132**, 1 (1986).
[10] M. Creutz, Phys. Rev. Lett. **50**, 1411 (1983).
[11] M. Falcioni, G. Martinelli, M. Paciello, G. Parisi, and B. Taglienti, Nucl. Phys. **B265**, 187 (1986).
[12] A. Gonzalez-Arroyo and M. Okawa, Phys. Rev. D **35**, 672 (1987).
[13] T. Banks, hep-th/0412129.
[14] P. Meisinger, T. Miller, and M. Ogilvie, Phys. Rev. D **65**, 034009 (2002).
[15] A. Dumitru, Y. Hatta, J. Lenaghan, K. Orginos, and R. D. Pisarski, Phys. Rev. D **70**, 034511 (2004).
[16] L. Dittmann, T. Heinzl, and A. Wipf, J. High Energy Phys. 06 (2004) 005.
[17] M. Billó, M. Caselle, A. D'Adda, and S. Panzeri, Nucl. Phys. **B472**, 163 (1996).
[18] *Handbook of Mathematical Functions*, edited by M. Abramowitz and I. Stegun (National Bureau of Standards, Washington, D.C., 1964).
[19] G. Roepstorff, *Path Integral Approach to Quantum Physics* (Springer, New York, 1994).
[20] Y. Fujimoto, H. Yoneyama, and A. Wipf, Phys. Rev. D **38**, 2625 (1988).
[21] L. O'Raifeartaigh, A. Wipf, and H. Yoneyama, Nucl. Phys. **B271**, 653 (1986).
[22] J. Polónyi and K. Szlachányi, Phys. Lett. B **110**, 395 (1982).
[23] A. Gocksch and M. Ogilvie, Phys. Rev. Lett. **54**, 1772 (1985).
[24] B. R. Moore and M. Ogilvie, Nucl. Phys. B Proc. Suppl. **17**, 350 (1990).
[25] M. Ogilvie, Phys. Rev. Lett. **52**, 1369 (1984).
[26] J. Drouffe, J. Jurkiewicz, and A. Krzywiecki, Phys. Rev. D **29**, 2982 (1984).
[27] F. Green and F. Karsch, Nucl. Phys. **B238**, 297 (1984).
[28] M. Gross and J. Wheater, Nucl. Phys. **B240**, 253 (1984).
[29] K. M. Bitar, S. A. Gottlieb, and C. K. Zachos, Phys. Rev. D **26**, 2853 (1982).
[30] A. Kennedy and B. Pendleton, Phys. Lett. B **156**, 393 (1985).
[31] K. Fabricius and O. Haan, Phys. Lett. B **143**, 459 (1984).
[32] T. R. Miller, available at http://hbar.wustl.edu/miller/.